Water Research 101 (2016) 555–563

Contents lists available at ScienceDirect

Water Research

journal homepage: www.elsevier.com/locate/watres

Photo-reduction of bromate in drinking water by metallic Ag and reduced graphene oxide (RGO) jointly modified $BiVO_4$ under visible light irradiation

Fei Chen [a, b], Qi Yang [a, b, *], Yu Zhong [a, b], Hongxue An [a, b], Jianwei Zhao [a, b], Ting Xie [a, b], Qiuxiang Xu [a, b], Xiaoming Li [a, b], Dongbo Wang [a, b, **], Guangming Zeng [a, b]

[a] College of Environmental Science and Engineering, Hunan University, Changsha, 410082, PR China
[b] Key Laboratory of Environmental Biology and Pollution Control, Hunan University, Ministry of Education, Changsha, 410082, PR China

ARTICLE INFO

Article history:
Received 29 January 2016
Received in revised form
29 May 2016
Accepted 3 June 2016
Available online 4 June 2016

Keywords:
Photo-reduction
BrO_3^-
$Ag@BiVO_4@RGO$
Visible light
Mechanism

ABSTRACT

Bromate (BrO_3^-), an oxyhalide disinfection by-product (DBP) in drinking water, has been demonstrated to be carcinogenic and genotoxic. In the current work, metallic Ag and reduced graphene oxide (RGO) co-modified $BiVO_4$ was successfully synthesized by a stepwise chemical method coupling with a photo-deposition process and applied in the photo-reduction of BrO_3^- under visible light irradiation. In this composite, metallic Ag acted as an electron donor or mediator and RGO enhanced the BrO_3^- adsorption onto the surface of catalysts as well as an electron acceptor to restrict the recombination of photo-generated electron-hole pairs. The $Ag@BiVO_4@RGO$ composite exhibited greater photo-reduction BrO_3^- performance than pure $BiVO_4$, $Ag@BiVO_4$ and $RGO@BiVO_4$ under identical experimental conditions: initial BrO_3^- concentration 150 μg/L, catalyst dosage 0.5 g/L, pH 7.0 and visible light ($\lambda > 420$ nm). The photoluminescence spectra (PL), electron-spin resonance (ESR), photocurrent density (PC) and electrochemical impedance spectroscopy (EIS) measurements indicated that the modified $BiVO_4$ enhanced the photo-generated electrons and separated the electron-hole pairs. The photocatalytic reduction efficiency for BrO_3^- removal decreased with the addition of electron quencher $K_2S_2O_8$, suggesting that electrons were the primary factor in this photo-reduction process. The declining photo-reduction efficiency of BrO_3^- in tap water should attribute to the consumption of photo-generated electrons by coexisting anions and the adsorption of dissolved organic matter (DOM) on graphene surface. The overall results indicate a promising application potential for photo-reduction in the DBPs removal from drinking water.

1. Introduction

Over the past decades, BrO_3^- originated from the chlorination or ozonation process in bromide-containing water has received a growing concern due to its carcinogenic and genotoxic properties (Von Gunten and Oliveras, 1998; Butler et al., 2005). The specified maximum contaminant level (MCL) of BrO_3^- for drinking water is 10 μg/L in the US and European countries (Wu et al., 2013; Weinberg et al., 2003), the same MCL is also explicitly stipulated in drinking water sanitary standard (GB 5749-2006) and drinking natural mineral water (GB 8537-2008) in China (Xu et al., 2012). To meet the strict limitation, the reduction of BrO_3^- to innocuous Br^- was proven to be efficient means. The reducing materials under study included biological activated carbon (Kirisits et al., 2001), ferrous ions (Chitrakar et al., 2011), zero-valent iron (Wang et al., 2009), layered double hydroxides (LDHs) (Zhong et al., 2013), activated carbon felt electrodes (Kishimoto and Matsuda, 2009) and Pd/Al_2O_3 catalyst (Chen et al., 2010). However, long reaction time, strict reaction condition and high risk to produce secondary pollutants limited the application of these reducing materials in practice, thus it is of a great necessity to develop a novel and economical alternative for bromate reduction.

Recently, photo-reduction technology has been implemented and emerged as a potential technology to remove BrO_3^- ions in drinking water (Zhang et al., 2010b; Peldszus et al., 2004). As a

* Corresponding author. College of Environmental Science and Engineering, Hunan University, Changsha, 410082, PR China.
** Corresponding author. College of Environmental Science and Engineering, Hunan University, Changsha, 410082, PR China.
E-mail addresses: feichen@hnu.edu.cn (F. Chen), yangqi@hnu.edu.cn (Q. Yang), w.dongbo@yahoo.com (D. Wang).

http://dx.doi.org/10.1016/j.watres.2016.06.006
0043-1354/

typical photocatalyst, TiO_2 and its related photocatalysts had been successfully used in bromate removal from water under UV irradiation (Noguchi et al., 2003). For example, Mills and his co-workers demonstrated that bromate ions in tap water were totally reduced by Pt/TiO_2 catalyst under UV irradiation of 254 nm (Mills et al., 1996). Huang et al. reported graphene-TiO_2 composite photocatalyst exhibited a higher photo-reduction capacity of BrO_3^- than pure TiO_2, because graphene as an acceptor enhanced the photo-generated electrons from the photo-excited P25 and increased the charge transportation (Huang et al., 2014). According to previous studies (Zhao et al., 2011), the primary reactions for modified TiO_2 (M-TiO_2) should be listed as follows:

$$\text{M-TiO}_2 + \text{UV} \rightarrow \text{M-TiO}_2\,(e^-) + \text{M-TiO}_2\,(h^+) \quad (1)$$

$$\text{M-TiO}_2\,(h^+) + OH^- \rightarrow \bullet OH \quad (2)$$

$$BrO_3^- + e^- + 6H^+ \rightarrow Br^- + 3H_2O \quad (3)$$

where electron (e^-) is a strong reducer, M-TiO_2 possessed better electron-hole pairs separation under UV light, as compared with pure TiO_2. It could be inferred that electrons played a vital role in the photo-reduction system and appropriate modifications to single-component photocatalyst might enhance the corresponding photocatalytic activity.

Considering the cost and convenience in practical application, numerous attempts were devoted to the exploration of visible-light photocatalyst. Monoclinic $BiVO_4$ (m-$BiVO_4$) with a band gap energy of 2.4 eV, responsible to visible light, has been found to be a perfect visible-light material for degradation of organic contaminants and purification of wastewaters (Park et al., 2013b; Rao et al., 2014; Zhong et al., 2011). A relatively low mobility of photo-generated charges for pure $BiVO_4$ hindered the separation of electron-hole pairs, presenting as an unsatisfactory photocatalytic activity (Jo et al., 2012). Appropriate modifications always could improve the separation of charge carriers for pure $BiVO_4$, the methods employed usually included: (I) heterojunction construction (Hong et al., 2011), (II) ions doping (Obregon and Colon, 2014), (III) morphologies control (Dong et al., 2014b), (IV) loading noble metal doping (Ge, 2008), and (V) interface effect (Li et al., 2015). Photo-oxidation mechanism via photo-generated holes and other oxidative active species ($\bullet O_2^-$ or $\bullet OH$) were majorly detected in current studies, while the research on the photo-reduction induced by electrons generated from $BiVO_4$ or modified $BiVO_4$ was fewer and the application of oxyhalide disinfection by-product (DBP) reduction was seldom reported.

Herein, reduced graphene oxide (RGO) was chosen as the substrate to support $BiVO_4$, owing to its unique two-dimensional carbon structure (sp2-hybridized type), excellent conductivity and large surface area (Zhang et al., 2010a, 2015). Highly conductive reduced graphene oxide could be regarded as the ideal co-catalysts to improve various semiconductor photocatalysts. RGO could not only serve as an excellent electron acceptor to restrict the recombination of photo-generated electron-hole pairs, but also adsorb a large volume of BrO_3^- on the surface of catalyst, which was regarded as the ideal co-catalysts to combine with other semiconductor photocatalysts. In addition, a small amount of metallic Ag co-doped photocatalysts were proven to be effective in oriented migration of photo-generated electrons. For example, Sun et al. successfully deposited Ag nanoparticles onto {101} facets of TiO_2 nanocrystals and possessed superior photocatalytic reduction activity to nitrate (Sun et al., 2016). Vanitha et al. fabricated a novel Ag decorated CeO_2/RGO as an efficient supercapacitor (Vanitha et al., 2015). For these reasons, metallic Ag and RGO were chosen to modify $BiVO_4$ in this study. The co-modified $BiVO_4$ overcame the common drawbacks of single-component photocatalyst and achieved higher charge-separation efficiency. Thus the photo-reduction of BrO_3^- under visible light over Ag@$BiVO_4$@RGO photocatalyst should be feasible and valuable. To the best of our knowledge, the relevant study has never been reported.

In this work, Ag@$BiVO_4$@RGO photocatalyst was fabricated through chemical deposition of RGO and photo-reduction of Ag nanoparticles on the surface of pre-prepared $BiVO_4$. The prepared composites were employed as photocatalyst to reduce BrO_3^- to Br^- under visible light irradiation. The effect of catalyst dosage, initial BrO_3^- concentrations, initial pH and different water sources were investigated in details. The generation and transfer of electrons and separation of electron-holes pairs during the whole photocatalytic processes were measured by PL, PC and EIS to elucidate the mechanism of how the prepared photocatalysts enhanced photo-reduction of BrO_3^-.

2. Experimental

2.1. Materials and photocatalysts preparation

All reagents were used as received without further treatments. De-ionized water (18.25 MΩ cm) from Millipore system was used throughout all the experiments. $BiVO_4$ was fabricated by a previously reported method with minor modifications (Booshehri et al., 2014). In a typical synthesis procedure: 6 mmol of $Bi(NO_3)_3\cdot H_2O$ was dissolved in 32 mL of HNO_3 (1 M). Afterwards the prepared NH_4VO_3 (keep the molar ratio of 1:1 with $Bi(NO_3)_3\cdot H_2O$) was added into the above solution. After being heated for 5 min and ultrasonicated for 40 min, $CO(NH_2)_2$ (3.0 g) was added and the resultant mixture was maintained at 80 °C for 24 h under oil bath condition. Finally, the product was collected by filtration, washed with de-ionized water and ethanol for several times and dried at 60 °C for 12 h.

The synthesis of RGO(1 wt%)/$BiVO_4$ was presented as follows: 0.006 g of grapheme oxide (GO) prepared according to modified Hummer's method (Gao and Wang, 2013) was dispersed into 50 mL of de-ionized water coupling with 2 h ultrasonic treatment. After that, 0.6 g of $BiVO_4$ was added and continuously stirred for 2 h under laboratory condition. Subsequently, 1 mL of $NH_3\cdot H_2O$ and 3 mL of N_2H_4 were added in sequence. After being stirred for 4 h at 80 °C under water bath condition, the resulting sample was centrifuged, washed and dried at 60 °C for 12 h. Furthermore, Ag(1.0 wt%)@$BiVO_4$@RGO was synthesized by a facile photo-reduction procedure. 0.25 g of $BiVO_4$@rGO and a certain amount (0.004 g) of $AgNO_3$ were dispersed into 10 mL de-ionized water. After that, 20 mL of methyl orange solution (20 mg/L) was added and kept 2 h stirring using a magnetic stirrer in the darkness. Then the mixture was exposed to a 300 W Xe lamp and irradiated for 1 h to photo-deposition of metallic Ag on the surface of $BiVO_4$@rGO. At last, the product was obtained by centrifugation, washing and vacuum drying.

2.2. Characterization

The as-prepared samples in the form of powder were collected and characterized by a Rigaku D/max 2500v/pc X-ray diffractometer with Cu Kα radiation at a scan rate of 0.1° 2θ s^{-1}. The XPS measurements were performed on a Thermo ESCALAB 250Xi spectrometer with Al Kα source. The photoluminescence (PL) spectra were recorded using a transient fluorescence spectrometer (Edinburgh FLsp920 full functional state). A zeta potential analyzer (Malvern) was used to measure the zeta potential of the samples under different pH conditions. Electron spin resonance (ESR) signals of spin-trapped paramagnetic species with 5, 5-dimethyl-l-

pyrroline N-oxide (DMPO) were detected using a Bruker ER200-SRC spectrometer under visible light irradiation (λ > 420 nm).

2.3. Photocatalytic activity test

In order to evaluate the photo-reduction performance of the as-prepared samples, photocatalytic removal of BrO_3^- ions were carried out under visible light irradiation using a 300 W Xe lamp (CEL-HXF300, China) with a 420 nm cut filter. The average light intensity striking the surface of reaction solution was about 100 mW cm^2. In a typical experiment, 0.03 g of photocatalysts were homogeneously dispersed into 60 mL of BrO_3^- solution (150 μg/L) by ultrasonic bath for 10 min. Another 20 min dark stirring at room temperature was maintained for achieving the adsorption-desorption equilibrium. After that, the mixture was exposed to visible light, and 3 mL of solution was taken out at given time interval, centrifuged by 8000 rpm/min, filtrated by 0.22 μm membrane filter and analyzed the residual BrO_3^- by an ion chromatograph system (Dionex ICS-900, USA) equipped with an AG-23 column with an AS-23 sampler.

2.4. Photo-electrochemical measurements

The photocurrent density (PC) and electrochemical impedance spectroscopy (EIS) spectra, were determined in a conventional three-electrode electrochemical cell with a working electrode, a platinum wire counter electrode and a saturated calomel electrode (SCE) as reference electrode. The working electrode was immersed in a sodium sulfate electrolyte solution (0.5 M) using CHI660C workstation and irradiated at a visible light. A 300 W Xe lamp served as the light source The average light intensity was about 100 mW cm^2. The available surface area of working electrodes for all photo-electrochemical tests was 0.25 cm^2.

3. Results and discussion

3.1. Characterization of as-prepared catalysts

The XRD patterns can provide information on the crystalline nature of the as-obtained photocatalysts, which are presented in Fig. S1 (Supplementary information). All patterns of samples exhibited sharp diffraction peaks, suggesting that high crystallinity was achieved. From Fig. S1A (Supplementary information), it could be deduced that all the peaks in the XRD pattern of $BiVO_4$ were indexed to monoclinic scheelite $BiVO_4$ phase (JCPDS File No. 14-0688) (Li et al., 2015). For Ag@$BiVO_4$, RGO@$BiVO_4$ and Ag@$BiVO_4$@RGO, no detectable diffraction peaks of silver species (38.1°, 44.2°, 64.4° and 77.4° for Ag (0) and 34.2° for Ag (1) (Liu et al., 2012) and RGO 2θ = 26° and 44° (Dong et al., 2014a) could be observed for the modified $BiVO_4$, possibly due to the relatively small dosage amount and low diffraction intensity of metallic Ag and RGO in the corresponding composites (Song et al., 2016). Fig. S1B (Supplementary information) showed the comparison of XRD patterns between the fresh and the used samples. No significant discrepancy was perceived in the crystal structure except the lower intensity of the XRD pattern after four cycles, validating high stability of Ag@$BiVO_4$@RGO under visible light irradiation.

The chemical states and the surface composition of Ag@$BiVO_4$@RGO composite powder were investigated by XPS analysis. Fig. S2A (Supplementary information) was a typical XPS survey spectrum of Ag@$BiVO_4$@RGO, which composed of Bi, O, V, Ag and C. Three characteristic peaks could be found in the high-resolution C 1s spectrum (Fig. S2B, Supplementary information). The peak located at 284.6 eV could be assigned to the sp2 bonded carbon (C-C) in graphene. The peak at 286.7 eV belonged to the oxygen containing functional groups (epoxy/hydroxyls, C—O) and while the peak appeared at 288.5 eV was associated with the O—C═O species (carboxyl) (Zhang et al., 2015). As depicted in Fig. S2C (Supplementary information), Ag 3d spectrum displayed two characteristic peaks at 368.3 eV and 374.4 eV, corresponding to Ag $3d_{5/2}$ and Ag $3d_{3/2}$, respectively (Song et al., 2016). The weight ratio of metallic Ag in the Ag@$BiVO_4$@RGO composite was calculated to be 0.95 wt% according to the XPS spectrum, which was in good consistence with the preparation (1 wt% of metallic Ag photo-deposition). Other elements (Bi, V and O) analyses could be found in Fig. S3 (Supplementary information). In addition, the surface areas of pure $BiVO_4$ and Ag@$BiVO_4$@RGO composite were measured by BET test (Fig. S4, Supplementary information). Compared to pure $BiVO_4$ (surface area = 33.625 m^2/g), Ag@$BiVO_4$@RGO nanocomposite displayed a higher surface area (64.321 m^2/g), validating that the presence of RGO on the surface of $BiVO_4$ resulted in higher surface area.

It is reported that the spectral absorption range would directly influence the number of photo-generated electrons and holes (Chen et al., 2016), so the optical absorption properties of pure $BiVO_4$ and modified $BiVO_4$ samples were investigated by UV—vis diffuse reflectance spectra (DRS). As displayed in Fig. S2D (Supplementary information), the bare $BiVO_4$ exhibited an absorption edge at ca. 517 nm with an edge band of 2.4 eV. An improved visible-light absorption capability was found in the presence of metallic Ag, RGO and the combination of two others on the surface of $BiVO_4$. The co-modified $BiVO_4$ (Ag@$BiVO_4$@RGO) presented the maximal visible-light absorption edge, which could be assigned to the grafting of RGO and the SPR effect of metallic Ag. The result demonstrated that the co-effect was an effective method to enhance the visible light performance of single semiconductor.

Moreover, the edge band calculation result of $BiVO_4$ was illustrated in Fig. S5 (Supplementary information). The band gap (E_g) of a semiconductor could be calculated by the following formula (Wang et al., 2015):

$$\alpha(h\nu) = A\left(h\nu - E_g\right)^{n/2} \quad (4)$$

where α, h, ν, E_g and A are indicative to the absorption coefficient, Planck constant, light frequency, band gap energy, and a constant, respectively. Among them, n is determined by the type of optical transition of a semiconductor ($n = 1$ and 4 for direct- and indirect-band-gap semiconductors, respectively). The n value for pure $BiVO_4$ was 4, and the corresponding energy band gap was measured to be about 2.4 eV.

3.2. Photo-reduction of BrO_3^- under visible light irradiation

In order to detect the photocatalytic performance of the as-prepared samples, experiments of BrO_3^- reduction were carried out under visible light irradiation. As shown in Fig. 1A, BrO_3^- concentrations decreased with the increasing irradiation time in the presence of pure $BiVO_4$ and modified $BiVO_4$ photocatalysts. Furthermore, it could be observed that modified $BiVO_4$ exhibited much superior photocatalytic activity than pure $BiVO_4$. Within the irradiation time of 120 min, BrO_3^- concentration decreased from 150 μg/L to 43 μg/L for pure $BiVO_4$, whereas it reduced to 12 μg/L and 2 μg/L for Ag@$BiVO_4$ and RGO@$BiVO_4$, respectively. Benefiting from the co-effect of Ag and RGO, BrO_3^- was almost reduced (99.1%) completely by Ag@$BiVO_4$@RGO composite in 90 min. Conversely, bromide concentrations in solution also increased with irradiation time. The total bromine contents maintained over 98% (Fig. S6, Supplementary information), suggesting that only photo-reduction process happened in the photocatalytic system.

The photo-reduction of BrO_3^- in this study followed the pseudo-first-order kinetic model. The rate constant (k) could be calculated

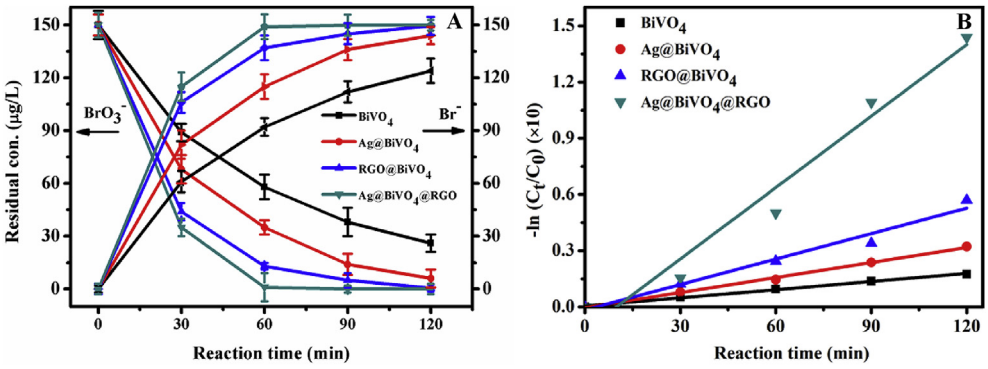

Fig. 1. Photo-reduction of BrO_3^- (A) and the corresponding rate constants (k) (B) over different as-prepared samples (Experimental conditions: initial BrO_3^- concentration 150 μg/L, catalyst dosage 0.5 g/L, reaction time 2 h, pH 7.0, reaction temperature 25 °C, light intensity 100 mW cm^2 (λ > 420 nm, 300 W Xe lamp)).

by the following equation (Zhong et al., 2013):

$$\ln (Ct/C0) = -kt \quad (5)$$

where C_0 and C_t are the concentration of BrO_3^- at the time of 0 and t, respectively (ug/L), and k represents the rate constant (min^{-1}). The corresponding plots of $-\ln(C_t/C_0)$~t exhibited a good linearity, and corresponding kinetic plots and first-order reactions parameters for pure $BiVO_4$ and modified $BiVO_4$ were distinctly depicted in Fig. 1B and Table 1, respectively. By considering the correlation coefficients (R^2), it could be found that the reduction of BrO_3^- over all prepared samples obeyed well the first-order reaction toward BrO_3^- concentrations ($R^2 > 0.97$). The rate constant over Ag@Bi-VO_4@RGO for the reduction of BrO_3^- was 0.1174 min^{-1}, which was as 8.1, 4.4 and 2.6 times higher than those reductions by pure $BiVO_4$, $Ag@BiVO_4$ and $Ag@BiVO_4$@RGO, respectively. Based on the above analysis, it could be concluded that photo-reduction of BrO_3^- under visible light by $BiVO_4$ was feasible and appropriate modifications were in favor of achieving better BrO_3^- removal efficiency. Table 2 presents some results of the previous studies on BrO_3^- reduction by photocatalysis, most of these procedures were concentrated on UV light field, leading to lower implementation possibility for practical application. Herein, $BiVO_4$ was perceived and a preferable BrO_3^- removal efficiency was attained under visible light irradiation. Moreover, the loading of Ag@RGO on the surface of $BiVO_4$ increased the conversion of BrO_3^- to Br^- to a greater extent by the improvement of electrons generating and transferring.

3.3. Effect of catalyst dosage

In view of economic condition, catalyst dosage was an important parameter for large-scale production. Results of residual BrO_3^- concentration in solutions against the amount of $Ag@BiVO_4$@RGO are depicted in Fig. 2A. A transparent trend distribution was found, the reduction ability firstly increased when the solid-to-solution ratio increasing from 0.167 g/L to 0.500 g/L, then decreased at 1.000 g/L and constantly declined at 1.667 g/L, suggesting an optimum catalyst dosage (0.500 g/L) existed in the photo-reduction procedure. Excess solid-to-solution ratio may lead to higher turbidity of the reaction system, resulting in worse light penetration through the BrO_3^- solution (Chen et al., 2016).

Table 1
Correlation coefficients and rate constants for the photo-reduction of BrO_3^- by the different as-prepared samples.

Catalyst	k (min^{-1})	R^2
$BiVO_4$	0.0145	0.995
$Ag@BiVO_4$	0.0267	0.997
$RGO@BiVO_4$	0.0452	0.978
$Ag@BiVO_4$@RGO	0.1174	0.972

3.4. Effect of initial concentrations

The effect of initial BrO_3^- concentration on the bromate removal by $Ag@BiVO_4$@RGO composite is displayed in Fig. 2B. When initial BrO_3^- concentrations increased from 100 μg/L to 300 μg/L, the corresponding BrO_3^- reduction efficiencies decreased. The reduction efficiency reached at 99.9% at the initial BrO_3^- concentration of 100 μg/L, whereas this value was only 33.6% at the concentration of 300 μg/L under identical condition. The same observation was also made in previous study (Wang et al., 2015). Lower photon adsorption on catalyst particles should be responsible for the missing photocatalytic activity along with higher initial concentrations. Meanwhile, lower photon entering resulted in less electrons generation among the photocatalytic process, further to obtain an unsatisfying BrO_3^- reduction. From Fig. 2B, almost similar variations of BrO_3^- removal at the initial concentration of 100 μg/L and 150 μg/L were distributed, thus we chose concentration of 150 μg/L as the target concentration of BrO_3^- for the remaining explorations.

3.5. Effect of initial pH

The influence of initial pH for BrO_3^- reduction by Ag@Bi-VO_4@RGO composite is presented in Fig. 2C. The reduction of BrO_3^- was highly dependent on the pH value and the highest reduction rate was obtained at pH 7.0. It was unsuitable for BrO_3^- removal under acidic and alkali conditions, as more H^+ or OH^- in the solution would play a negative role in the photo-reduction process. Deep insight into the zeta potential of as-synthesized Ag@Bi-VO_4@RGO (Table 3), potential became more negative with the increasing of initial pH values. The ξ-potentials at given pH values 3, 5, 7, 9, and 11 were 3.24 mV, -15.32 mV, -25.48 mV, -37.25 mV and −46.32 mV, respectively. As the pH was lowered, the functional groups were protonated and the corresponding proportion of the positive-charged surface increased. In basic condition, less BrO_3^- was adsorbed on the surface of the catalyst due to the intrinsic repulsion between the anions and the negative surface of Ag@Bi-VO_4@RGO by OH^- adsorption, indicating that less BrO_3^- could be reduced attributing to the less contacting probability. Furthermore, the generated active species (OH·, hydroxyl radical) also lead to the oxidation of Br^-, which was in accordance with the previous finding (Park et al., 2013a; Von Gunten and Oliveras, 1998). The reactions between hydroxide ions and positive holes brought out

Table 2
Summary of photocatalytic reduction of BrO_3^- ions over previous studies.

Catalyst	Light source (nm)	Catalysis dosage (g/L)	BrO_3^- concentration (μg/L)	pH	*k* for pseudo-first-order (10^{-3} min^{-1})	Reference
Pt/TiO_2	UV(254)	0.4	50	8.1	9.3	(Mills et al., 1996)
Pseudo-BM/TiO_2	UV(365)	0.2	200	7.0	4.1–9.2	(Noguchi et al., 2003)
TiO_2	UV(365)	0.5	128	1.5–13.5	6.2	(Zhang et al., 2010b)
C60/Bi_2MoO_6	Vis(>420)	0.83	30	7.0	3.4–10.0	(Zhao et al., 2011)
RGO/TiO_2	UV(254)	0.1	10,000	5.1–9.2	9.4–21.0	(Huang et al., 2014)
Ag@RGO@$BiVO_4$	Vis (>420)	0.5	150	3.0–11.0	15–117	In this study

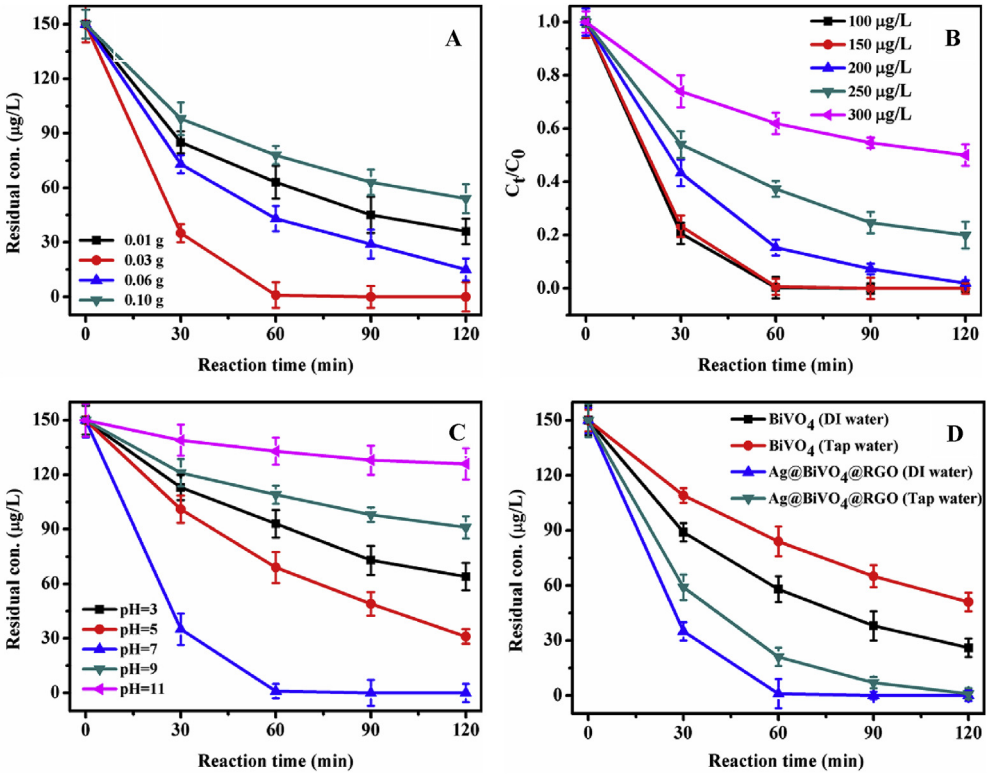

Fig. 2. Effect of catalysis dosage (A) (Experimental conditions: initial BrO_3^- concentration 150 μg/L, reaction time 2 h, pH 7.0, reaction temperature 25 °C, light intensity 100 mW cm^2 (λ > 420 nm, 300 W Xe lamp)); initial BrO_3^- concentrations (B) (Experimental conditions: catalyst dosage 0.5 g/L, reaction time 2 h, pH 7.0, reaction temperature 25 °C, light intensity 100 mW cm^2 (λ > 420 nm, 300 W Xe lamp)); initial pH (C) (Experimental conditions: initial BrO_3^- concentration 150 μg/L, catalyst dosage 0.5 g/L, reaction time 2 h, reaction temperature 25 °C, light intensity 100 mW cm^2 (λ > 420 nm, 300 W Xe lamp)); and water sources (D) (Experimental conditions: initial BrO_3^- concentration 150 μg/L, catalyst dosage 0.5 g/L, reaction time 2 h, pH 7.0, reaction temperature 25 °C, light intensity 100 mW cm^2 (λ > 420 nm, 300 W Xe lamp)) on the reduction of BrO_3^- by Ag@$BiVO_4$@RGO composite.

Table 3
The ξ-potentials and bromate reduction efficiency of Ag@$BiVO_4$@RGO composite at different initial pH.

pH[a]	3	5	7	9	11
ξ-potential (mV)	3.24	−15.32	−25.48	−37.25	−46.32
Bromate reduction efficiency[b]	56.7%	81.5%	99.1%	38.4%	16.3%

[a] The pH was pre-adjusted with 0.1 mol/L H_2SO_4 and 0.1 mol/L NaOH.
[b] Reaction conditions: initial BrO_3^- concentration 150 μg/L, catalyst dosage 0.5 g/L, reaction time 2 h, pH 7.0, reaction temperature 25 °C, light intensity 100 mW cm^2 (λ > 420 nm, 300 W Xe lamp).

the forming of oxidation species. As for the reduction process in acidic condition, more electrons could transfer to the surface of Ag@$BiVO_4$@RGO composite because of the autogenous attraction. As a result, the reduction efficiency in acidic condition was much better than that in basic condition. However, the increasing H^+ could react with OH^-, oxidation species such as ($HO_2\cdot$) could be formed and promoted the process of oxidation Br^- to BrO_3^- (Huang et al., 2014), leading to a relative low BrO_3^- removal efficiency. According to the above-mentioned analysis, the optimum reduction condition could be observed at a neutral solution (pH 7.0), it was unbeneficial for degradation reaction of BrO_3^- reduction predominantly ascribed to the formed oxidation radicals or less BrO_3^- adsorption under acidic or basic condition.

3.6. Photo-reduction of BrO_3^- in tap water

The photo-reduction of BrO_3^- by pure $BiVO_4$ and Ag@$BiVO_4$@RGO composite was also examined with the tap water originated from Xiang River and de-ionized water, respectively. As clearly illustrated in Fig. 2D, preferable BrO_3^- removal efficiencies by Ag@$BiVO_4$@RGO was achieved in both water sources, verifying that metallic Ag and RGO co-modified $BiVO_4$ exhibited a desirable reduction property in natural water. Nevertheless, the BrO_3^- removal in tap water was inhibited to some extent. The BrO_3^- removal efficiency in de-ionized water could achieve 99.1% within the irradiation time of 90 min, while it needed 120 min to reach the same effect for tap water. The similar phenomenon was found for

Table 4
The corresponding compositions in the tap water originated from Xiang River.

Parameter	Value
pH	7.7 ± 0.23%
DO	8.9 ± 2.02%
COD (mg/L)	45 ± 3.86%
Chloride (mg/L)	18.8 ± 3.05%
Sulfate (mg/L)	28.4 ± 3.52%
NH_3-N (mg N/L)	0.016 ± 4.32%
Nitrate (mg N/L)	0.086 ± 3.24%
Nitrite (mg N/L)	0.048 ± 2.59%
Bromide (μg/L)	12.5 ± 2.82%
Bromate (μg/L)	0.5 ± 3.82%

pure $BiVO_4$ sample, the residual concentration of BrO_3^- in de-ionized water (43 μg/L) was obviously lower than that in tap water (67 μg/L) after photocatalytic reduction. Based on the concrete composition in tap water (Table 4), it could be deduced that the competitive anions such as NO_3^-, NO_2^- might consume photo-generated electrons, therefore BrO_3^- reduction was hampered. On the other hand, natural organic matters (NOMs) in tap water could also impact the transporting or transferring of electrons between reduced graphene oxide and $BiVO_4$ (Huang et al., 2014). The dissolved organic matters (DOMs) were absorbed by RGO prior to BrO_3^- ions, resulting in less electrons in the photocatalytic system. Thus an adequate pre-treatment should be added for better reduction efficiency of BrO_3^-.

3.7. The photocatalytic stability of Ag@$BiVO_4$@RGO

The photo-stability was a critical property for photocatalyst in practical application. Fig. 3A depicted the typical time course for BrO_3^- reduction by Ag@$BiVO_4$@RGO composite at four consecutive runs. After each run, the catalyst was washed by de-ionized water and ethanol, and retested in the fresh BrO_3^- (150 μg/L) under the same experimental conditions as previous mentioned. It could be noticed that there were no significant loss for the reduction ability of BrO_3^- during the cycles, suggesting that Ag@$BiVO_4$@RGO composite possessed high photo-stability in repeated use.

3.8. Proposed photo-reduction mechanism in BrO_3^- removal

For better understanding the enhancement of photocatalytic activity as well as the detailed degradation process by Ag@$BiVO_4$@RGO composite, it is pivotal and necessary to discuss the intrinsic reaction mechanism. Enhanced production of photo-generated electrons and separation of electron-hole pairs were proposed responsible for superior photo-reduction property, and a series of characterization methods (ESR, PL, PC and EIS) were adopted to ascertain our speculation.

The previous study had confirmed that electrons preferred to react with $S_2O_8^{2-}$ other than BrO_3^- (Zhao et al., 2011), thus the introduction of $K_2S_2O_8$ was a marker to analyze the major species in the reduction process. To determine the role of electron in the photo-reduction process, $K_2S_2O_8$ was employed and added into the solution with the catalyst. The test results in Fig. 3B were in good consistence with the hypothesis, the efficiency of BrO_3^- removal significantly decreased with the addition of $K_2S_2O_8$. Along with the increasing amount of the quencher, the photo-reduction process was hindered to a greater extent, and almost restrained with 8 mmol $K_2S_2O_8$. (only 2.1% of BrO_3^- was reduced). It could be recognized that electrons should be responsible for the reduction of BrO_3^- ions.

DMPO spin-trapping technology was introduced to further investigate the role of electrons in the photo-reduction process of BrO_3^- removal over Ag@$BiVO_4$@RGO composite. As depicted in Fig. 4A, the characteristic peak of DMPO-•O_2^- adduct was observed for pure $BiVO_4$ and Ag@$BiVO_4$@RGO composite under visible light irradiation, but the characteristic peak did not find at dark condition. Thus, the •O_2^- was proven to be generated in the photocatalytic process. The peak intensity of the DMPO-·O_2^- adduct for Ag@$BiVO_4$@RGO composite was much higher than that of pure $BiVO_4$, suggesting that Ag@$BiVO_4$@RGO promoted the production of electrons. Furthermore, in order to exclude the adverse effect of •O_2^- for BrO_3^- reduction, parallel experiments were carried out under air and N_2 atmosphere, respectively (Fig. S7, Supplementary information). It could be seen that the reduction process was promoted under N_2 atmosphere, due to the inhibition role for the production of oxidation species •O_2^-. It had been suggested that 2,2,6,6-Tetramethylpiperidinooxy (TEMPO) could also be used as a spin label for indirect detecting the electrons generated among photocatalytic process. The ESR spectra of TEMPO aqueous solution all displayed two stable signal peaks with catalysts or without catalysts before irradiation. In this study, the same signal intensities were achieved for the as-prepared samples at dark condition. After 4 min of visible-light irradiation, the signal intensity for Ag@$BiVO_4$@RGO was much lower than that of pure $BiVO_4$ (Fig. 4B), indicating that more electrons were produced in the presence of Ag@$BiVO_4$@RGO and revealed with a better photo-reduction performance (He et al., 2014; Zhang et al., 2005). The above-mentioned results validated that more photo-induced electrons were

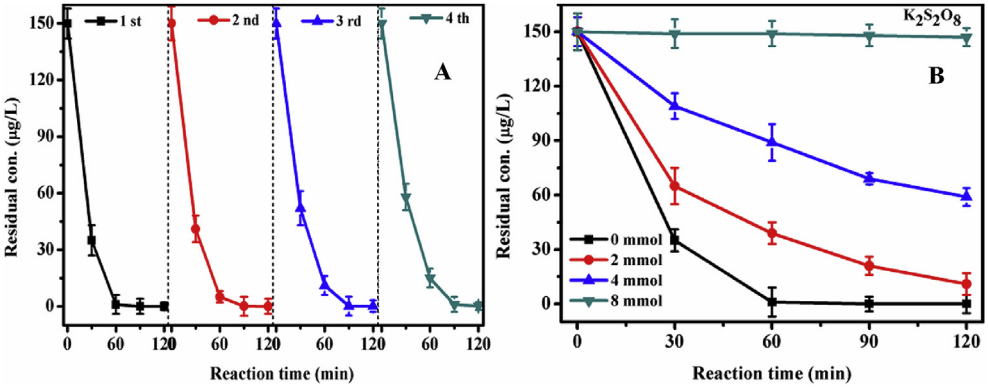

Fig. 3. Photo-reduction of BrO_3^- at four successive cycles (A) and effect of $K_2S_2O_8$ (B) on the reduction of BrO_3^- by Ag@$BiVO_4$@RGO composite under visible light irradiation. (Experimental conditions: initial BrO_3^- concentration 150 μg/L, catalyst dosage 0.5 g/L, reaction time 2 h, pH 7.0, reaction temperature 25 °C, light intensity 100 mW cm^2 (λ > 420 nm, 300 W Xe lamp)).

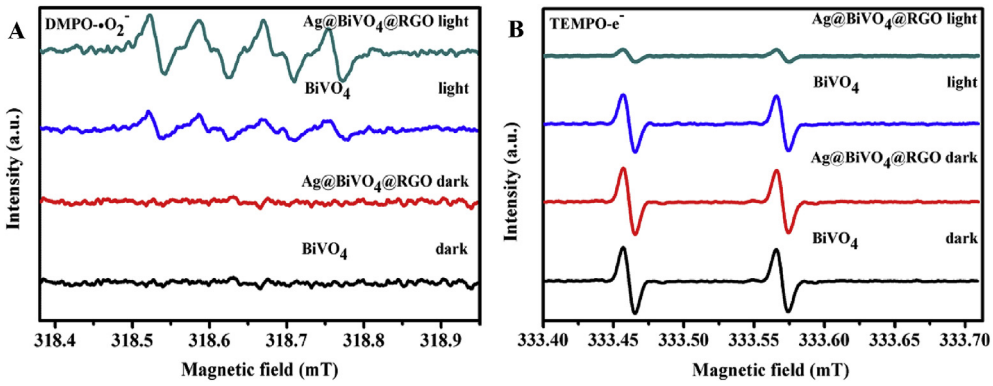

Fig. 4. DMPO spin-trapping ESR spectra of $BiVO_4$ and Ag@$BiVO_4$@RGO in methanol dispersion for DMPO-$\cdot O_2^-$ in dark or under visible light irradiation (A); ESR spectra of $BiVO_4$ and Ag@$BiVO_4$@RGO containing TEMPO aqueous solution for e^- detection after 4 min of visible light irradiation or in dark (B).

generated over Ag@$BiVO_4$@RGO nanocomposite.

The PL emission intensity is an indicative of electron-hole separation efficiency, which is often used to explore the charge carrier trapping, migration and transfer (Wang et al., 2016). As seen in Fig. 5A, Ag@$BiVO_4$@RGO composite exhibited the lowest PL intensity in comparison with pure $BiVO_4$, Ag@$BiVO_4$ and RGO@$BiVO_4$, which implied that the recombination of electron-hole pairs was restricted effectively for the co-effect of metallic Ag and reduced graphene oxide.

To obtain the transient photo-response of pure $BiVO_4$, Ag@$BiVO_4$, RGO@$BiVO_4$ and Ag@$BiVO_4$@RGO, photocurrent density were measured under illumination with several cycles of 20 s intervals light on or off in 0.5 M Na_2SO_4 solution. Larger photocurrent indicated a higher electrons and holes separation efficiency (Wang et al., 2016). As illustrated in Fig. 5B, it was worth noticing that the photo-current density of Ag@$BiVO_4$@RGO composite electrode (2.68 μA cm^{-2}) was 3.7 times higher than that of pure $BiVO_4$ (0.72 μA cm^{-2}), 2.5 times of Ag@$BiVO_4$ (1.08 μA cm^{-2}) and 1.6 times of RGO@$BiVO_4$ (1.64 μA cm^{-2}). The results demonstrated that metallic Ag and RGO co-modified $BiVO_4$ possessed higher separation efficiency of photo-generated electron-hole pairs and a lower recombination rate of charge carriers. The superior photo-electric reproducibility of Ag@$BiVO_4$@RGO will greatly exploit its potential application in other fields, such as photodector, solar cell and so on.

In this study, the transfer and migration processes of the photo-generated electron-hole pairs were revealed by electrochemical impedance spectra (EIS). The arc radius on the EIS Nyquist plot has been used to investigate the reaction rate occurring at the surface of the as-prepared working electrodes (Li et al., 2015; Wang et al.,

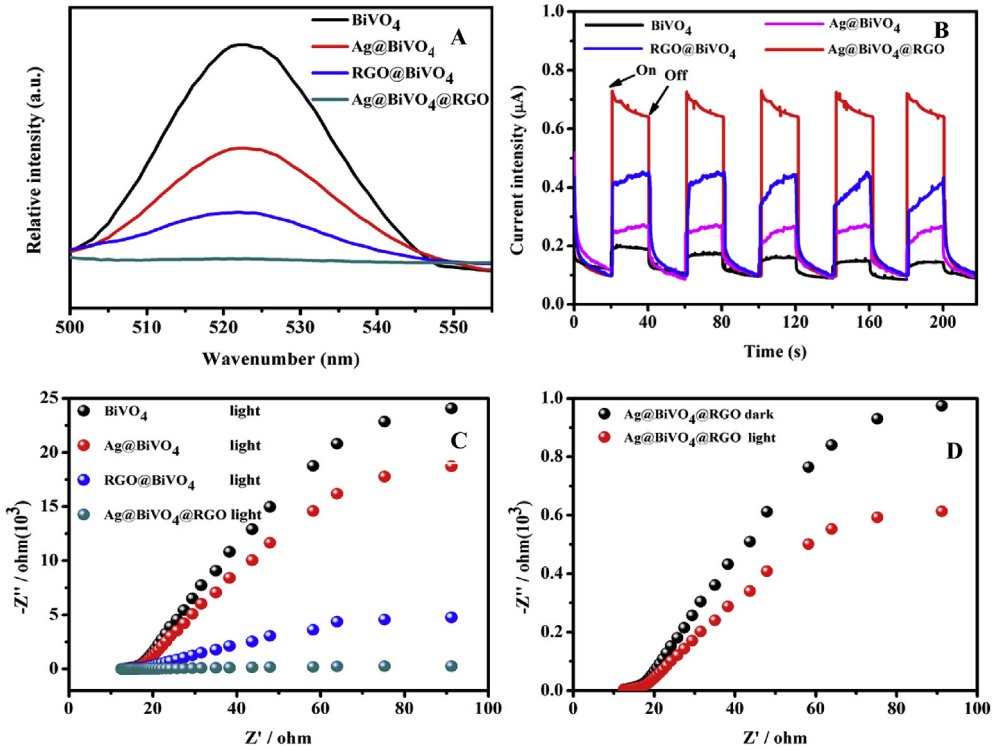

Fig. 5. Photoluminescence spectra (A), photocurrent density (B) over all the as-prepared samples and EIS (C) for different catalyst film electrodes under visible light irradiation, and EIS (D) for Ag@$BiVO_4$@RGO under visible light and dark condition respectively.

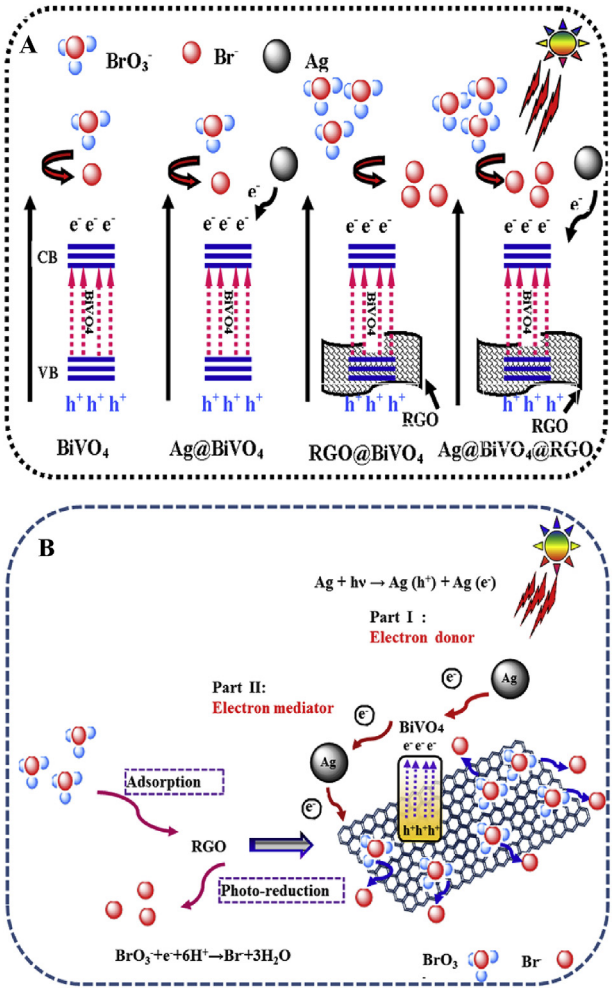

Fig. 6. Schematic diagram: possible photocatalytic mechanism of pure $BiVO_4$ and modified $BiVO_4$ (A) and detailed charge transfer and photo-reduction processes for Ag@$BiVO_4$@RGO composite (B).

2016). As depicted in Fig. 5C, the diameter of arc radius of pure $BiVO_4$, Ag@$BiVO_4$, $BiVO_4$@RGO and Ag@$BiVO_4$@RGO appeared a trend of diminishing under visible light irradiation. The Nyquist arc radius diameter of Ag@$BiVO_4$@RGO was the minimum, demonstrating that the reaction rate on the electrode surface was the fastest and the electrode resistance was the smallest, so the separation efficiency of photo-generated electrons and holes over Ag@$BiVO_4$@RGO composite was the highest. Meanwhile, Ag@$BiVO_4$@RGO exhibited a smaller diameter under visible light than in the darkness (Fig. 5D), which should be attributed to the generation of photo-excited carriers under visible light condition.

On the basis of the results described above, the possible mechanism for BrO_3^- reduction by Ag@$BiVO_4$@RGO composite was proposed and illustrated in Fig. 6. Metallic Ag played an important role in two aspects, electron donor and electron mediator, under visible light irradiation. Ag nanoparticles could absorb the incident photons and produced electrons and holes attributable to the surface plasmon resonance (SPR) induced electronic field (Sun et al., 2016; Li et al., 2015). The photo-generated electrons from Ag particles could be transformed to the conduction band of $BiVO_4$, resulting in electron-deficient Ag and a lower recombination rate of photo-generated electrons and holes. In addition, metallic Ag was served as an electron mediator in the reduction procedure. The electrons on the CB of $BiVO_4$ could be quickly transferred to the conduction band of RGO with the help of Ag transporter. Through such way, photo-generated electrons were effectively formed and transported in whole reduction process, presenting as superior electron-hole pairs separation efficiency and enhancement in photocatalytic activity. Owing to the large surface area and electron storage, more BrO_3^- could be absorbed on the surface of RGO and the accumulated electrons could commendably react with the target electron acceptor BrO_3^-. Furthermore, a small amount of Ag might be switched into Ag^+, then free Ag^+ in the system which combined with the product Br^- and emerged as AgBr. The photo-reduction performance could be enhanced ascribed to the forming heterojunction between AgBr and $BiVO_4$ with higher electron-hole pairs separation. Generally speaking, noble Ag functioned as electron donor coupling with electron mediator, leading to plentiful electrons formed and facilitating the charge transfer process simultaneously. The reduced graphene oxide worked as an effective platform for BrO_3^- absorption and provided enough electrons for BrO_3^- reduction. Consequently, in the presence of metallic Ag and RGO, co-modified $BiVO_4$ could acquire excellent production, transportation and mobility of electrons, revealing highly improved photo-reduction performance for BrO_3^- removal.

4. Conclusions

In this study, novel visible-light photocatalyst of Ag@$BiVO_4$@RGO was fabricated by a facile chemical and photo-deposition process. The coupling effects of metallic Ag and RGO prompted a satisfying photocatalytic activity over modified $BiVO_4$, realizing the high charge-separation efficiency as well as long-term stability. The corresponding photocatalytic performance was evaluated by photo-reduction of BrO_3^- under visible light irradiation. After 90 min, 99.1% of BrO_3^- was removed by Ag@$BiVO_4$@RGO composite with catalyst dosage 0.5 g/L and pH 7.0, which was 8.1, 4.4 and 2.6 times higher than those of $BiVO_4$, Ag@$BiVO_4$, RGO@$BiVO_4$, respectively. Substantial improvement of photo-generated electrons production and electron-hole pairs separation was verified by ESR, PL, PC and EIS measurements. The introduction of metallic Ag played a crucial role in electron generation as well as RGO acted as an electron accepter and enhanced the adsorption of target pollutant. Compared with the reduction process in de-ionized water, there was a significant loss for BrO_3^- removal by Ag@$BiVO_4$@RGO composite in tap water originated from Xiang River. The competitive anions consumed the electrons and other natural organic matters adsorption on the surface of RGO, resulting in lower BrO_3^- reduction efficiency. New insight into metallic Ag and RGO co-modified $BiVO_4$ for BrO_3^- reduction under visible light illumination may provide a more comprehensive potential for other disinfection byproducts removal in drinking water. Possible applications in other fields, such as photodector, solar cell and so on, owing to its superior photoelectric properties of Ag@$BiVO_4$@RGO composite.

Acknowledgments

This research was financially supported by the project of National Natural Science Foundation of China (NSFC) (Nos. 51378188, 51478170, 51508178), Doctoral Fund of Ministry of Education of China (20130161120021) and Planned Science and Technology Project of Hunan Province, China (No. 2015SK20672).

Appendix A. Supplementary information

Supplementary information related to this article can be found at http://dx.doi.org/10.1016/j.watres.2016.06.006.

References

Booshehri, A.Y., Goh, S.C., Hong, J.D., Jiang, R.R., Xu, R., 2014. Effect of depositing silver nanoparticles on $BiVO_4$ in enhancing visible light photocatalytic inactivation of bacteria in water. J. Mater. Chem. A 2 (17), 6209–6217.

Butler, R., Godley, A., Lytton, L., Cartmell, E., 2005. Bromate environmental contamination: review of impact and possible treatment. Crit. Rev. Environ. Sci. Technol. 35 (3), 193–217.

Chen, F., Yang, Q., Niu, C.G., Li, X.M., Zhang, C., Zhao, J.W., 2016. Enhanced visible light photocatalytic activity and mechanism of $ZnSn(OH)_6$ nanocubes modified with AgI nanoparticles. Catal. Commun. 73, 1–6.

Chen, H., Xu, Z., Wan, H., Zheng, J., Yin, D., Zheng, S., 2010. Aqueous bromate reduction by catalytic hydrogenation over Pd/Al_2O_3 catalysts. Appl. Catal. B 96 (3), 307–313.

Chitrakar, R., Sonoda, A., Makita, Y., Hirotsu, T., 2011. Synthesis and bromate reduction of sulfate intercalated Fe(II)-Al(III) layered double hydroxides. Sep. Purif. Technol. 80 (3), 652–657.

Dong, S.Y., Cui, Y.R., Wang, Y.F., Li, Y.K., Hu, L.M., Sun, J.Y., Sun, J.H., 2014a. Designing three-dimensional acicular sheaf shaped $BiVO_4$/reduced graphene oxide composites for efficient sunlight-driven photocatalytic degradation of dye wastewater. Chem. Eng. J. 249, 102–110.

Dong, S.Y., Feng, J.L., Li, Y.K., Hu, L.M., Liu, M.L., Wang, Y.F., 2014b. Shape-controlled synthesis of $BiVO_4$ hierarchical structures with unique natural-sunlight-driven photocatalytic activity. Appl. Catal. B 152, 413–424.

Gao, E.P., Wang, W.Z., 2013. Role of graphene on the surface chemical reactions of $BiPO_4$-rGO with low OH-related defects. Nanoscale 5 (22), 11248–11256.

Ge, L., 2008. Novel visible-light-driven $Pt/BiVO_4$ photocatalyst for efficient degradation of methyl orange. J. Mol. Catal. A 282 (1), 62–66.

He, W., Kim, H.K., Wamer, W.G., Melka, D., Callahan, J.H., Yin, J.J., 2014. Photogenerated charge carriers and reactive oxygen species in ZnO/Au hybrid nanostructures with enhanced photocatalytic and antibacterial activity. J. Am. Chem. Soc. 136 (2), 750–757.

Hong, S.J., Lee, S., Jang, J.S., Lee, J.S., 2011. Heterojunction $BiVO_4/WO_3$ electrodes for enhanced photoactivity of water oxidation. Energy Environ. Sci. 4 (5), 1781–1787.

Huang, X., Wang, L.Y., Zhou, J.Z., Gao, N.Y., 2014. Photocatalytic decomposition of bromate ion by the UV/P25-graphene processes. Water Res. 57, 1–7.

Jo, W.J., Jang, J.W., Kong, K., 2012. Phosphate doping into monoclinic $BiVO_4$ for enhanced photoelectrochemical water oxidation activity. Angew. Chem. Int. Ed. 51 (13), 3147–3151.

Kirisits, M.J., Snoeyink, V.L., Inan, H., Chee-sanford, J.C., Raskin, L., Brown, J.C., 2001. Water quality factors affecting bromate reduction in biologically active carbon filters. Water Res. 35 (4), 891–900.

Kishimoto, N., Matsuda, N., 2009. Bromate ion removal by electrochemical reduction using an activated carbon felt electrode. Environ. Sci. Technol. 43 (6), 2054–2059.

Li, H.Y., Sun, Y.J., Cai, B., Gan, S.Y., Han, D.X., Niu, L., 2015. Hierarchically Z-scheme photocatalyst of Ag@AgCl decorated on BiVO4 (040) with enhancing photoelectrochemical and photocatalytic performance. Appl. Catal. B 170, 206–214.

Liu, H., Cao, W.R., Su, Y., Wang, Y., Wang, X.H., 2012. Synthesis, characterization and photocatalytic performance of novel visible-light-induced Ag/BiOI. Appl. Catal. B 111, 271–279.

Mills, A., Belghazi, A., Rodman, D., 1996. Bromate removal from drinking water by semiconductor photocatalysis. Water Res. 30 (9), 1973–1978.

Noguchi, H., Nakajima, A., Watanabe, T., Hashimoto, K., 2003. Design of a photocatalyst for bromate decomposition: surface modification of TiO_2 by pseudoboehmite. Environ. Sci. Technol. 37 (1), 153–157.

Obregon, S., Colon, G., 2014. Heterostructured Er^{3+} doped $BiVO_4$ with exceptional photocatalytic performance by cooperative electronic and luminescence sensitization mechanism. Appl. Catal. B 158, 242–249.

Park, H., Park, Y., Kim, W., Choi, W., 2013a. Surface modification of TiO_2 photocatalyst for environmental applications. J. Photochem. Photobiol. C 15, 1–20.

Park, Y., McDonald, K.J., Choi, K.S., 2013b. Progress in bismuth vanadate photoanodes for use in solar water oxidation. Chem. Soc. Rev. 42 (6), 2321–2337.

Peldszus, S., Andrews, S.A., Souza, R., Smith, F., Douglas, I., Bolton, J., Huck, P.M., 2004. Effect of medium-pressure UV irradiation on bromate concentrations in drinking water, a pilot-scale study. Water Res. 38 (1), 211–217.

Rao, P.M., Cai, L., Liu, C., 2014. Simultaneously efficient light absorption and charge separation in $WO_3/BiVO_4$ core/shell nanowire photoanode for photoelectrochemical water oxidation. Nano Lett. 14 (2), 1099–1105.

Song, S.Q., Cheng, B., Wu, N.S., Meng, A.Y., Cao, S.W., Yu, J.G., 2016. Structure effect of graphene on the photocatalytic performance of plasmonic Ag/Ag_2CO_3-rGO for photocatalytic elimination of pollutants. Appl. Catal. B 181, 71–78.

Sun, D.C., Yang, W.Y., Zhou, L., Sun, W.Z., Lia, Q., Shang, J.K., 2016. The selective deposition of silver nanoparticles onto {101} facets of TiO_2 nanocrystals with co-exposed {001}/{101} facets and their enhanced photocatalytic reduction of aqueous nitrate under simulated solar illumination. Appl. Catal. B 182, 85–93.

Vanitha, M., Cao, P., Balasubramanian, N., 2015. Ag nanocrystals anchored CeO_2/graphene nanocomposite for enhanced supercapacitor applications. J. Alloys Compd. 644, 534–544.

Von Gunten, U., Oliveras, Y., 1998. Advanced oxidation of bromide-containing waters: bromate formation mechanisms. Environ. Sci. Technol. 32 (1), 63–70.

Wang, H., Yuan, X.Z., Wu, Y., Zeng, G.M., 2015. Synthesis and applications of novel graphitic carbon nitride/metal-organic frameworks mesoporous photocatalyst for dyes removal. Appl. Catal. B 174, 445–454.

Wang, P., Li, X., Fang, J.L., Li, D.Z., Chen, J., Zhang, X.Y., 2016. A facile synthesis of CdSe quantum dots-decorated anatase TiO_2 with exposed {001} facets and its superior photocatalytic activity. Appl. Catal. B 181, 838–847.

Wang, Q., Snyder, S., Kim, J., Choi, H., 2009. Aqueous ethanol modified nanoscale zerovalent iron in bromate reduction: synthesis, characterization, and reactivity. Environ. Sci. Technol. 43 (9), 3292–3299.

Weinberg, H.S., Delcomyn, C.A., Unnam, V., 2003. Bromate in chlorinated drinking waters: occurrence and implications for future regulation. Environ. Sci. Technol. 37 (14), 3104–3110.

Wu, X.Q., Yang, Q., Xu, D.C., Zhong, Y., Luo, K., Li, X.M., 2013. Simultaneous adsorption/reduction of bromate by nanoscale zerovalent iron supported on modified activated carbon. Ind. Eng. Chem. Res. 52 (35), 12574–12581.

Xu, C., Shi, J., Zhou, W., Gao, B., Yue, Q., Wang, X., 2012. Bromate removal from aqueous solutions by nano crystalline akaganeite (-FeOOH)-coated quartz sand (CACQS). Chem. Eng. J. 187, 63–68.

Zhang, F.X., Jin, R.C., Chen, J.X., Shao, C.Z., Gao, W.L., Li, L.D., Guan, N.J., 2005. High photocatalytic activity and selectivity for nitrogen in nitrate reduction on Ag/TiO_2 catalyst with fine silver clusters. J. Catal. 232 (2), 424–431.

Zhang, H., Guo, L.H., Wang, D.B., Zhao, L.X., Wan, B., 2015. Light-induced efficient molecular oxygen activation on a Cu(II)-grafted TiO_2/graphene photocatalyst for phenol degradation. ACS Appl. Mater. Inter. 7 (3), 1816–1823.

Zhang, L.L., Xiong, Z.G., Zhao, X.S., 2010a. Pillaring chemically exfoliated graphene oxide with carbon nanotubes for photocatalytic degradation of dyes under visible light irradiation. ACS Nano 4 (11), 7030–7036.

Zhang, X., Zhang, T., Ng, J., Pan, J.H., Sun, D.D., 2010b. Transformation of bromine species in TiO_2 photocatalytic system. Environ. Sci. Technol. 44 (1), 439–444.

Zhao, X., Liu, H.J., Shen, Y.L., Qu, J.H., 2011. Photocatalytic reduction of bromate at C60 modified Bi_2MoO_6 under visible light irradiation. Appl. Catal. B 106 (1), 63–68.

Zhong, D.K., Choi, S., Gamelin, D.R., 2011. Near-complete suppression of surface recombination in solar photoelectrolysis by "Co-Pi" catalyst-modified W: $BiVO_4$. J. Am. Chem. Soc. 133 (45), 18370–18377.

Zhong, Y., Yang, Q., Luo, K., Wu, X.Q., Li, X.M., Liu, Y., Tang, W.W., Zeng, G.M., 2013. Fe(II)-Al(III) layered double hydroxides prepared by ultrasound-assisted co-precipitation method for the reduction of bromate. J. Hazard. Mater. 250, 345–353.